3D printed spherical mini-tablets: Geometry versus composition effects in controlling dissolution from personalised solid dosage forms

Sejad Ayyoubi[a,b], Jose R. Cerda[a], Raquel Fernández-García[a], Peter Knief[c], Aikaterini Lalatsa[d], Anne Marie Healy[e], Dolores R. Serrano[a,f*]

[a] Department of Pharmaceutics and Food Science, Facultad de Farmacia, Universidad Complutense de Madrid, 28040, Madrid, Spain.

[b] School of Pharmacy, Utrecht University, Universiteitsweg 99, 3584 CG Utrecht, The Netherlands.

[c] UCD Centre for Precision Surgery, Catherine McAuley Education and Research Centre, Dublin 7, Ireland.

[d] Biomaterials, Bio-engineering and Nanomedicine (BioN) Lab, Institute of Biomedical and Biomolecular Sciences, School of Pharmacy and Biomedical Sciences, University of Portsmouth, White Swan Road, Portsmouth PO1 2 DT, U. K.

[e] SSPC The SFI Research Centre for Pharmaceuticals, School of Pharmacy and Pharmaceutical Sciences, Trinity College Dublin, Dublin 2, Ireland

[f] Instituto de Farmacia Industrial y Galénica, School of Pharmacy, Universidad Complutense de Madrid, 28040, Madrid, Spain.

Corresponding author:

Dolores R. Serrano
Department of Pharmaceutics and Food Science
School of Pharmacy
Universidad Complutense de Madrid
Email: drserran@ucm.es
Tel: +34 91 394 1620

This is a peer-reviewed, accepted author manuscript of the following article: Ayyoubi, S., Cerda, J. R., Fernández-García, R., Knief, P., Lalatsa, A., Healy, A. M., & Serrano, D. R. (2021). 3D printed spherical mini-tablets: geometry versus composition effects in controlling dissolution from personalised solid dosage forms. International Journal of Pharmaceutics, 597, [120336]. https://doi.org/10.1016/j.ijpharm.2021.120336

Abstract

Oral dosage forms are by far the most common prescription and over-the-counter pharmaceutical dosage forms used worldwide. However, many patients suffer from adverse effects caused by their use of "one-size fits all" mass produced commercially available solid dosage forms, whereby they do not receive dedicated medication or dosage adjusted to their specific needs. The development of 3D printing paves the way for personalised medicine. This work focuses on personalised therapies for hypertensive patients using nifedipine as the model drug. 3D printed full solid and channelled spherical mini-tablets with enhanced surface area (1.6-fold higher) were printed using modified PVA commercial filaments loaded by passive diffusion (PD), and Kollidon VA64 (KVA) and ethylcellulose (EC) based filaments prepared by hot-melt extrusion (HME). Drug loading ranged from 3.7% to 60% based on the employed technique, with a 13-fold higher drug loading achieved with the HME compared to PD. Composition was found to have a more significant impact on drug dissolution than geometry and surface area. Both KVA and EC-based formulations exhibited a biphasic zero-order drug-release profile. Physicochemical characterization revealed that nifedipine was in the amorphous form in the KVA-based end-products which led to a greater dissolution control over a 24 h period compared to the EC-based formulations that exhibited low levels of crystallinity by PXRD. The proposed 3D printed spherical mini-tablets provide a versatile technology for personalised solid dosage forms with high drug loading and dissolution control, easily adaptable to patient and disease needs.

Keywords: 3D printing, Fused Deposition Modelling (FDM), mini-tablets, hot-melt extrusion (HME), nifedipine

Graphical abstract

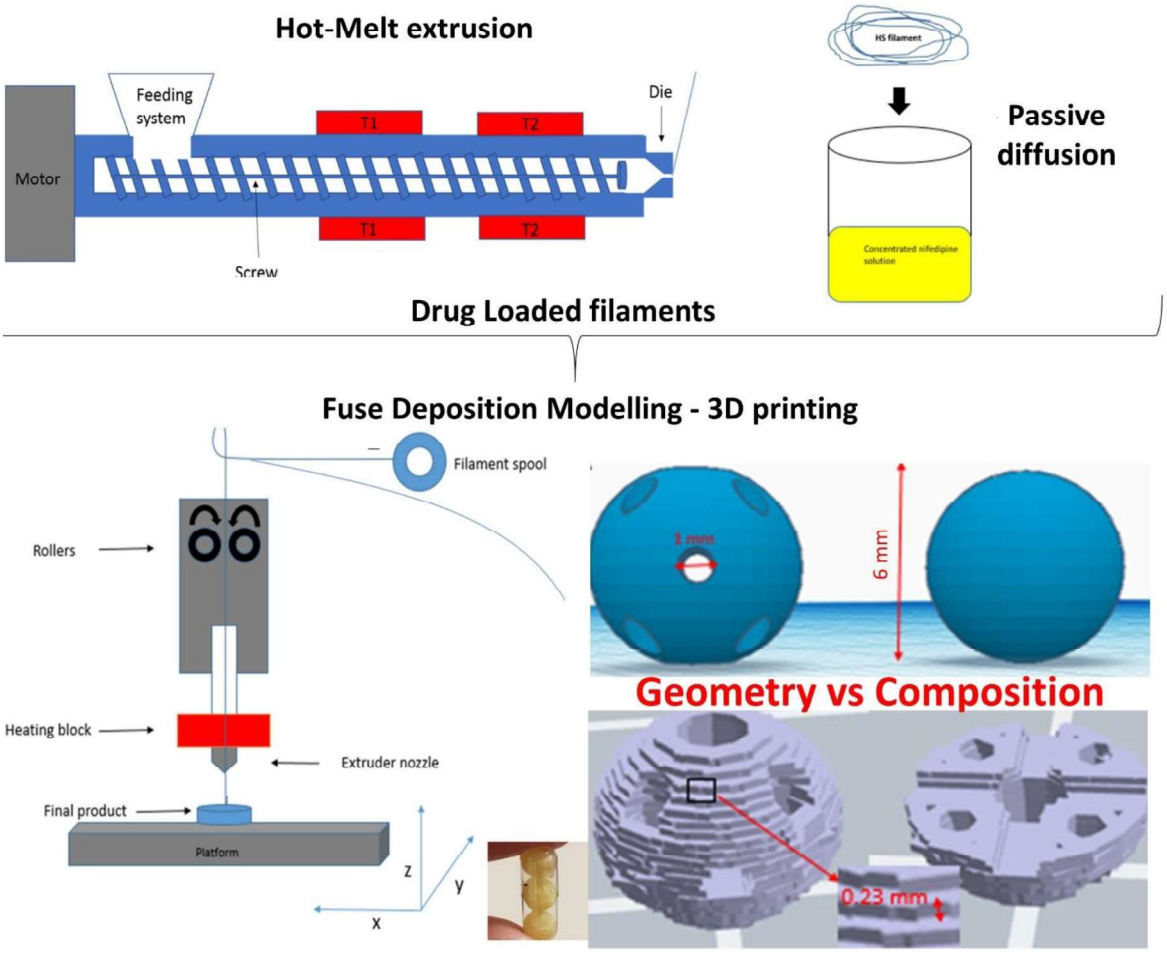

1. Introduction

The ideal scenario for healthcare would be for all patients to receive personalised pharmacotherapy based on the patient's profile [such as age, weight, genetic and pharmacokinetic profile (e.g. eGFR)] and disease characteristics (such as co-morbidities) instead of a 'one size fits all' treatment (Harvey et al., 2012). The development of new techniques, such as 3D printing (3DP), in the field of pharmaceutical technology paves the way for personalised medicine, as 3D printed medicines are unique formulations that can be adapted to patients' needs (Awad et al., 2018a). Some of the advantages of 3D printed medicines include control of the dose in an accurate manner (Skowyra et al., 2015), and the ability to incorporate multiple active pharmaceutical ingredients (API) into one dosage form that can result in enhanced adherence in cancer (Serrano et al., 2019b) and polymedicated patients (Khaled et al., 2015). The release profiles of each individual API within a specific formulation can also be defined (Fina et al., 2020; Gioumouxouzis et al., 2020; Khaled et al., 2015; Pereira et al., 2020; Tan et al., 2019). Lastly, modification of colour, taste, and geometry of 3D printed medicines is also possible (Konta et al., 2017). Overall, 3D printed personalised medicines can lead to greater patient compliance, better pharmacotherapy, and thus to safer and more effective health outcomes (Januskaite et al., 2020; Konta et al., 2017; Serrano et al., 2019a). 3D printing has also been used in novel applications, such as printing of medicines with unique designs (Isreb et al., 2019), opioid medicines with alcohol-resistant and abuse-deterrent properties (Nukala et al., 2019; Ong et al., 2020), and also as an anti-counterfeit measurement for personalised products (Trenfield et al., 2019).

From the seven 3D printing categories described by the American Society for Testing and Materials (ASTM), the most commonly used techniques in 3D printing of medicines are: binder jetting, vat photopolymerisation, including stereolithography and digital light processing, and material extrusion processes, including fused deposition modelling (FDM), which utilises thermoplastics, and semisolid extrusion (SSE), based on the use of gels and pastes (Awad et al., 2018b). Ensuring the appropriate 3DP method is selected for the intended API is critical to avoid manufacturing and technical issues. With FDM technology (a nozzle based deposition system), high temperatures are used during printing, in order to melt the mixture of API and excipients (Konta et al., 2017). There are several FDM 3D printers, but with a similar mechanism of action (Fig 1A). The printing resolution with an FDM printer ranges from 0.05-0.5 mm (Femmer et al., 2016). However, due to the high temperatures required for FDM, it is less suitable for thermolabile drugs. The low availability of thermoplastic materials with good melt viscosity for extrusion remains another limitation (Konta et al., 2017) and the development of suitable filaments for FDM is key to the success of this technique.

Filaments can be engineered either by hot-melt extrusion (HME) or by passive diffusion after immersion in a saturated solution containing the API (Cerda et al., 2020). For the latter approached, commercial filaments can be used for first drug loading and then printing. A wide variety of filaments with unique properties are on the market, although none that are loaded with drugs are yet approved for pharmaceutical use. It is also possible to create specific and unique filaments with different ratios of API/excipients through HME (Tiwari et al., 2016). A hot-melt extruder consists of a feeding system, one or two screws, a heating system and an

extruder head with an orifice which gives shape to the extrudate (Fig. 1B) (Maniruzzaman et al., 2012; Wilson et al., 2012). Powder combinations of API-excipients can be inserted in the feeding system after which the screw pushes the mixture towards the extruder head. Before reaching the extruder head, the mixture melts as it passes the heating system. The melted mixture eventually reaches the die and hardens outside of the extruder, obtaining a defined filament ideally with the correct diameter to be fed into the FDM printer.

HME allows for the manufacture of high drug loaded filaments (Verstraete et al., 2018). The formation of amorphous solid dispersions during the melting process, can lead to an improved water-solubility and oral bioavailability of poorly soluble APIs, as well as control of API release from the polymeric matrix (Tiwari et al., 2016). A suitable miscible combination of API(s) with low glass transition temperature (T_g) polymers, such as polycaprolactone, can lead to a reduction of the overall melting temperature of the powder mixture and hence, reduces the risk of API degradation by high temperatures. The challenge with HME remains to create a 'printable' filament with the correct diameter, rheological properties, mechanical strength, and elastic modulus to avoid blockages during printing (Elbadawi et al., 2020a; Elbadawi et al., 2020b; Nasereddin et al., 2018). As an alternative, direct powder extrusion has emerged as a new technology to avoid the need for creating a printable filament (Fanous et al., 2020; Goyanes et al., 2019; Ong et al., 2020).

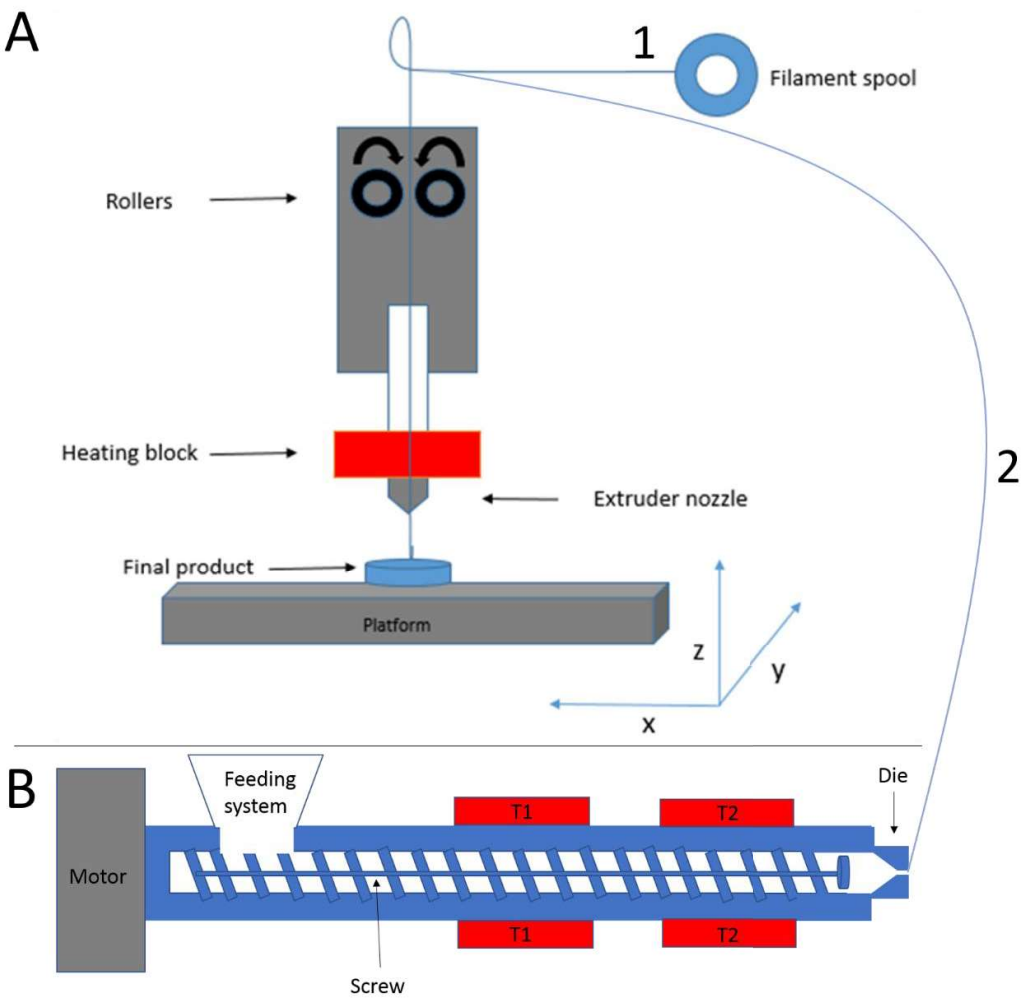

Figure 1: Schematics of FDM 3D printing (A) and Hot melt extrusion (B).

On the other hand, passive diffusion is a drug loading method based on the immersion of prefabricated filaments in an API saturated solution. This method is easy, but requires highly potent drugs where low drug loadings are adequate, as drug loading does not typically exceed 2% of API within the filaments (ranging from 0.06% w/w to 1.9% w/w) (Goyanes et al., 2014; Goyanes et al., 2015a; Skowyra et al., 2015). However, recent studies indicate that the application of the Hansen solubility theory to understand which polymer and solvent combination is more suitable has allowed filaments with higher drug loadings to be obtained by passive diffusion (≥ 3%) (Cerda et al., 2020).

Here, we have chosen a calcium channel blocker, nifedipine (NFD), a BCS class II agent, mainly used for the management of hypertension and angina pectoris (Gajendran et al., 2015) as a model drug. NFD is a suitable model drug for 3D printing considering that dose adjustment is essential for proper management of hypertension and only a limited range of doses are commercially available. NFD has good permeability and low aqueous solubility (Gajendran et

al., 2015), and is a photolabile drug with a melting point of 172–174 °C (Da Silva Leite et al., 2013). The oral bioavailability of nifedipine is variable due to its low solubility (Cavallari et al., 2016). Personalised 3D printed NFD formulations are not yet available and the challenge is to ensure that the formulations meet the regulatory agencies requirements, while at the same time remain patient friendly oral dosage forms that can improve the patient's quality of life. Here we have manufactured mini-tablets as flexible personalised dosage forms loaded with NFD using FDM 3D printing. Mini-tablets allow for facile dose adjustments as well as the ability, if required, to combine different APIs loaded in different tablets within the same capsule in order to avoid physicochemical interactions. We have designed spherical mini-tablets with different geometries with enhanced surface area and with different compositions to investigate the impact of these parameters on the final characteristics of the 3DP solid dosage forms utilising either commercially available filaments loaded by passive diffusion (PD) or in-house manufactured filaments prepared using HME based on different polymer compositions. The impact of geometry design on the drug release profile was explored by designing and printing channelled mini-tablets for the first time with a 1.6-fold higher surface area than tablets without channels. The physicochemical characteristics of the manufactured 3DP mini-tablets were finally tested and compared in terms of content uniformity, morphology, thermal properties, drug loading, and dissolution characteristics.

2. Materials and methods

2.1.Materials

NFD was purchased from Industria Chimica Italiana (>95%, Bergamo, Italia). PEG 4000 and magnesium stearate were purchased from Sigma–Aldrich (Madrid, Spain). Hydrosupport filaments with 1.75 mm diameter (>96% polyvinyl alcohol and polyethylene glycol) was a gift from 3D-Fuel (Donegal, Ireland). Klucel hydroxypropyl cellulose (HPC) grade LF and Aqualon ethylcellulose (EC) N10 were kindly donated by Ashland (Madrid, Spain). Kollidon VA 64 (KVA64) was purchased from BASF (Ludwigshafen, Germany). Size 0 hard gelatine capsules were a gift from Capsugel (Madrid, Spain). Adalat OROS 30 mg (Bayer, Leverkusen, Germany) and nifedipine retard 20 mg tablets (Stada, Bad Vilbel, Germany) were included as commercialised formulations for comparison purposes. The composition of Adalat OROS coated tablet is polyethylene oxide, hypromellose, magnesiusm stearate, sodium chloride, cellulose acetate, macrogol, hydroxypropyl cellulose and propylene glycol, while the generic uncoated nifedipine retard tables are comprised of microcrystalline cellulose, maize starch, monohydrate lactose, polysorbate 80, magnesium stearate, hypromellose, macrogol 4000, titanium oxide. Any other reagents were used without further purification.

2.2.Methods

2.2.1. Preparation of NFD loaded filaments

Passive diffusion

Based on preliminary solubility studies, a saturated solution of NFD in ethanol was prepared (30 mg/ml). Hydrosupport filaments (1 m in length and 1. 75 mm in diameter) were completely immersed in the saturated solution (100 ml) for 8 hours at room temperature to allow the NFD to passively diffuse into the filament. Previous studies have shown that NFD exhibited the highest diffusion rate across hydrosupport filaments compared with rigid polyvinyl alcohol and rigid poly lactic acid commercial filaments (Cerda et al., 2020). Diffusion times greater than 8 hours led to chemical degradation of NDF in solution and consequently to a lower drug loading. After 8 hours, the filament was dried in an oven at 40 ºC overnight to ensure evaporation of the ethanol, followed by drying at 100 ºC for an extra hour prior to printing at room temperature in order to increase the mechanical strength of the filaments and facilitate the printing process (Cerda et al., 2020).

HME

Mixtures of NFD, Aqualon EC N10, PEG 4000, magnesium stearate (MgS), Kollidon VA 64 (KVA64) and Klucel HPC LF were extruded into filaments by HME for subsequent 3D printing with FDM. The different compositions prepared at 20 g batch sizes were extruded at different temperatures as detailed in Table 1. EC, HPC and KVA64 were used to create a defined release polymeric matrices. PEG 4000 was included as plasticiser, and magnesium stearate as lubricant to promote the homogenous transit of the powder mixture through the extruder. Ball milling (IKA Ultra-Turrax® Tube Drive Disperser) was used to blend the feed powder mixture for 2 min at 6,000 rpm after which the mixture was sieved through a 12-US mesh (1.68 mm) screen prior to extrusion. HME of the mixture was performed with a Noztek touch single-screw extruder (Shoreham, UK) at 30 rpm.

Table 1: Compositions of HME formulations and extrusion temperatures for the manufacture of the NFD filaments. The "cp" annotations in the formulation code stand for "channelled Mini-tablet".

	Composition (%, w/w)						Extrusion zone temperature (ET)	
Formulation code	**NFD**	**EC**	**HPC**	**PEG 4000**	**MgS**	**KVA64**	**First ET (T1) (ºC)**	**Second ET (T2) (ºC)**
1 (EC30)	30	20	44	5	1	0	110	165
2 (EC40)	40	10	44	5	1	0	110	165
3 (EC50)	50	10	34	5	1	0	110	165
4 (cpEC50)	50	10	34	5	1	0	110	165
5 (EC60)	60	10	24	5	1	0	110	165
6 (cpPKVA150)	50	0	34	5	1	10	0	155
7 (KVA250)	50	0	24	5	1	20	0	145

2.2.2. 3D FDM printing

Geometry design

The Mini-tablet geometry was designed using a computer-aided design (CAD) software (Tinkercad software v.1, Autodesk 2019, Barcelona, Spain) to create a .stl file compatible with the Flashprint software v.4.6.0. (Flashprint, Flashforge, Zhejiang Flashforge 3D Technology Co, Zhejiang, China) to adjust the printing parameters (Fig. 2). Mini-tablets were designed with spherical shape with a diameter of 6 mm in order to fit within a size 0 hard capsule. The total surface area of each mini-tablet was calculated using Meshlab v.1.5.2. (Visual Computing Laboratory, CNR-ISTI, Italy) to be 133.1 mm^2.

Channelled mini-tablets were also engineered with the aim of increasing the surface area that was exposed to the dissolution media. Three channels were designed into the 6 mm tablet in all the three axes: Y, X and Z. The Y channel was 2 mm in diameter while the other two channels were 1 mm in diameter to maintain the structural integrity of the mini-tablet. In addition, four lateral channels (with a diameter of 1 mm) were also incorporated in each quarter of the tablet. A schematic design of the final geometry is illustrated in Figure 2. Based on the calculations of Meshlab software, the surface area of the channelled mini-tablets was increased by 1.6-fold (221.8 mm^2) relative to the original non-porous/non-channelled tablets.

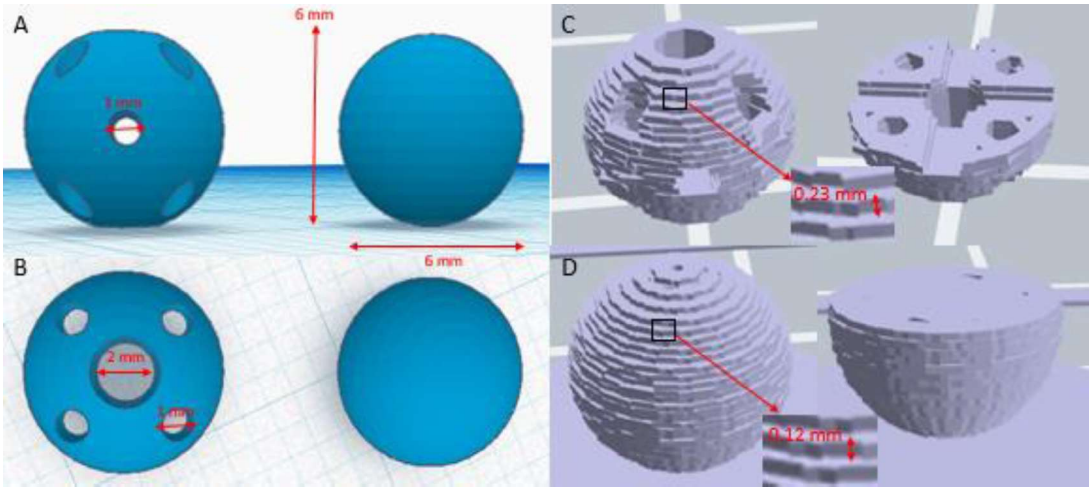

Figure 2. Geometric design of the solid and channelled mini-tablet of NFD formulations. A) Lateral CAD view; B) Top CAD view (Tinkercad software v.1); C) Sliced model of channelled Mini-tablet and D) Sliced view of full infill Mini-tablet (Flashprint software v.4.6.0.).

FDM printing settings and geometry design

A FlashForge Creator Pro (Zhejiang Flashforge 3D Technology Co, Zhejiang, China) FDM 3D printer was used to print the mini-tablets. The platform temperature was set at 50 °C and the printing temperature was set at 223 °C for all formulations. NFD degradation was minimal at this temperature (corroborated by TGA, Fig 6). Lastly, the print and travel speed were both set at 10 mm/s. Other relevant settings are summarised in Table 2 for all formulations.

Table 2: Printing settings for all NFD formulations. Key:*cp: channelled mini-tablet. The infill of all tablets was 100%.

Formulation	Layer height (mm)	First layer (mm)
PD	0.12	0.20
1 (EC30)	0.23	0.23
2 (EC40)	0.23	0.23
3 (EC50)	0.23	0.23
4 (cpEC50)*	0.23	0.23
5 (EC60)	0.23	0.23
6 (cpKVA150)*	0.12	0.20
7 (KVA250)	0.12	0.20

2.2.3. Content uniformity and drug loading

Drug loading in mini-tablets and filaments was assessed for the PD formulation and for the EC50 formulation. Mini-tablets (n=10) obtained by passive diffusion were dissolved in mobile phase consisting of (methanol: water: acetonitrile (36:55:9, v:v)) and mini-tablets obtained from HME filaments were dissolved in acetonitrile. All the samples were then diluted in mobile phase prior to quantification by HPLC.

2.2.4. Dissolution studies

Dissolution tests were performed in triplicate using a United States Pharmacopoeia (USP) apparatus 2 (ERWEKA DT 80, Heusenstamm, Germany) at 100 rpm (United States Pharmacopeia and National Formulary, USP38-NF33). The employed dissolution media were: USP simulated gastric fluid (SGF) without enzymes (pH 1.2) with 0.5% sodium lauryl sulfate and USP simulated intestinal fluid (SIF) without enzymes (pH 6.8) with 0.5% sodium lauryl sulfate as described in the USP (United States Pharmacopeia and National Formulary (USP 38-NF 33). Reagents: Test Solutions. Rockville). SGF (400 ml) was used during the first 2 hours. SIF (500 ml) was added and kept for the remaining 22 hours and media were maintained at 37 ± 0.5 °C. NaOH (30% v/v) was used to adjust the pH to 6.8 after the addition of the SIF. Samples (2 ml) were withdrawn from the dissolution media and filtered through a hydrophilic 0.45 µm filter (Millipore, Millex-LCR, Massachusetts, US) at 5, 10, 15, 30 and 45 minutes 1, 1.5, 2, 3, 4, 6 and 24 hours. Samples were diluted with mobile phase (1:2 v/v) consisting of methanol: water: acetonitrile (36:55:9, v:v), and subsequently analysed by HPLC comprised of

a Jasco PU-1580 pump, a Jasco AS-2050 Plus autosampler and a Jasco UV-1575 UV-visible detector. Integration of the peaks was performed with Borwin 1.5 software. NFD was separated on a Thermo BDS Hypersil C18 reverse-phase column (200 x 4.6 mm, 5 µm). The mobile phase was pumped at a flow rate of 1 mL/min and the sample injection volume was 20 µL. The column temperature was kept at 25º C and the detector was set at 240 nm. The detection limit was 0.12 µg/mL while the quantification limit was 0.4 µg/mL (Cerda et al., 2020).

The dissolution data obtained were fitted using the following kinetic equations (Costa and Sousa Lobo, 2001; Siepmann and Siepmann, 2013): zero order (Eq. 1), first order (Eq. 2), Hixson–Crowell (Eq. 3), Korsmeyer–Peppas (Eq. 4) and Higuchi (Eq. 5):

$$Q_t = Q_0 + K_0 t \qquad (Eq.\ 1)$$

$$LogQ_t = logQ_0 + K_1 t 2.303 \qquad (Eq.2)$$

$$W_0^{1/3} - W^{1/3}_t = K_s t \qquad (Eq.\ 3)$$

$$Log(Mt/M\infty) = log\ K_{kp} + nlogt \qquad (Eq.\ 4)$$

$$Q = tDC_s(2C-C_s) \qquad (Eq.\ 5)$$

where Q_t is the amount of drug dissolved in time t, Q_0 is the initial amount of drug in the solution (most times, $Q_0 = 0$), W_0 is the initial amount of drug in the tablet, W_t is the remaining amount of drug in the tablet; $Mt/M\infty$ is the fraction of drug release at time t; D is the diffusion constant, C is the initial drug concentration, C_s is the drug solubility in the matrix medium and Q is the amount of drug release per time, t, per unit area; K_1 is the first order release constant, K_0 is the zero order release constant, K_s is a constant incorporating the surface-volume relation; K_{KP} is a constant that describes the structural and geometric characteristics of the drug dosage form; n is the release exponent which describes the drug release mechanism. The n has a value of 0.5, 0.45 or 0.43 when the particle shape is a thin film, a cylinder or a sphere respectively which indicates Fickian release controlled by diffusion (Serrano et al., 2016). Anomalous non-Fickian transport is observed when n is between those values and 1 ($0.5 < n < 1$ for thin films, $0.45 < n < 1$ for cylinder and $0.43 < n < 1$ for spheres). Values of n=1 correspond to zero order release (Lao et al., 2011). The choice of release profile that best fits the release data is determined based on the obtained regression coefficient (R^2) (Costa and Sousa Lobo, 2001; Mamani et al., 2012; Serrano et al., 2016).

2.2.5. Scanning Electron Microscopy (SEM)

A scanning electron microscope (JSM 6335F JEOL, Japan) was used at 15.0 kV, after the samples were sputtered coated with pure gold (Q150RS Metalizador QUORUM, UK) for 180 seconds. Micrographs were obtained from filaments, 100% fully printed mini-tablets and tablets printed only up to 50% of the total geometry in order to investigate the geometry of the core.

2.2.6. Friability and hardness testing

A friability test (Pharmatest PTF friability tester, Hainburg, Germany) at 100 rotations and a hardness test (Pharmatest PTB 311, Hainburg, Germany) was undertaken for the mini-tablets according to the USP (United States Pharmacopeia and National Formulary (USP 38-NF 33). General Chapters: <1216> TABLET FRIABILITY. Rockville; United States Pharmacopeia and National Formulary (USP 38-NF 33). General Chapters: <1217> TABLET BREAKING FORCE. Rockville). The tests were performed with the PD formulation (n=10) and for the EC50 formulation (n=10).

2.2.7. Solid state characterisation

Solid state characterisation was performed on 3D printed filaments and mini-tablets, unprocessed excipients and nifedipine. Physical mixtures between drug and excipients were prepared in an agate mortar and pestle and were also analysed. A thin slice (1-2 mm) of the 3D printed filaments and mini-tablets was cut with a small cutter and analysed to avoid grinding.

Fourier-transform infrared (FTIR) spectroscopy

FTIR analysis of printed mini-tablets was carried out with a Luminar 5030 Spectrometer (Brimrose, America). The following settings were used: wavelength range 1100 – 2300 cm^{-1}, 10 scans, and detector gain of 2 (except when analysing raw NFD powder, in which a detector gain of 1 was used). Spectragryph (version 1.2.9, Oberstdorf, Germany) software was used for the interpretation of the spectra.

X-ray powder diffraction (pXRD)

Powder X-ray analysis was performed using a Miniflex II Rigaku diffractometer with Ni-filtered Cu Kα radiation (1.54 Å). The tube voltage and tube current used were 30 kV and 25 mA, respectively. The PXRD patterns were recorded (n=3) from 5° to 40° on the 2 theta scale at a step scan rate of 0.05° per second (Serrano et al., 2016). Full mini-tablets and filaments were loaded in an open holder to avoid altering the PXRD signal by grinding (n=3). The NFD PXRD peak used was at 16.6 2θ degrees, which was selected due to the lack of interference with other peaks in the diffractogram. Rigaku Peak Integral software was used for the determination of the peak intensity for each sample using the Sonnefelt-Visser background edit procedure.

Modulated temperature DSC (MTDSC)

MTDSC scans were recorded on a QA-200 TA instrument (TA instruments, Elstree, UK) calorimeter using nitrogen as the purge gas. A section of the mini-tablets and filaments was cut, weighed (4-6 mg) and sealed in an open aluminium pan. A scanning rate of 5 °C/min, amplitude of modulation of 0.796 °C and modulation frequency of 1/60 Hz were employed. The temperature range was set between 10 °C to 200 °C (Serrano et al., 2018). Calibration of the instrument was carried out using indium as standard. Glass transition temperatures reported (n = 3) are the midpoint of the transition.

Thermogravimetric analysis (TGA)

Thermogravimetric analysis (TGA) was performed using a Q-50 TA instrument (TA instruments, Elstree, UK). Samples were placed in open aluminium pans (2-6 mg) and analyses were performed at a constant heating rate of 10°C/min between a temperature range of 25 °C and 300 °C (Rolon et al., 2017).

Dynamic Vapour Sorption (DVS)

Water sorption kinetic profiles were obtained using DVS (Advantage, Surface Measurement Systems, Alperton, UK) at 25.0 ± 0.1°C for the EC50 and KVA250 formulations. Water was used as the probe vapour. Samples were dried at 0% relative humidity (RH) for 1 h and then subjected to step changes of 10% RH up to 90% RH, and the reverse for desorption. The sample mass was allowed to reach equilibrium, defined as dm/dt ≤0.002 mg/min over 10 min, before the RH was changed. Sample weights were between 70 and 80 mg corresponding to one whole mini-tablet to avoid altering the structure.

Data processing and statistical analysis

Statistical analysis for the dissolution study data was performed via one-way ANOVA test using Minitab v.16 (Minitab Ltd, Coventry, UK) followed by Tukey's test considering p-values for statistical significance to be below 0.05. Linear regression analysis was performed using the method of least squares by Microsoft® Excel 2010 software (Microsoft Corporation, Redmond, WA, USA). The adequacy of the fit was assessed based on the regression coefficient (R^2). Comparison and modelling of dissolution curves were undertaken using the mathematical software DDsolver (China Pharmaceutical University, Nanjing, China) (Zhang et al., 2010). Dissolution results were plotted using Microsoft® Excel 2010 software. A multivariate data analysis was performed using The Unscrambler® X software (CAMO Software, Oslo, Norway) in order to assess the influence of the excipients on the NFD release using dissolution study data (Matji et al., 2019). A principal component analysis (PCA), a partial least square (PLS) analysis, and a multilinear regression (MLR) were performed based on the dissolution data.

3. Results

3.1. Filament manufacturing and morphology

The morphology of all formulations is illustrated in Fig 3 & 4. The appearance of the PD mini-tablets showed a very smooth surface with minimal printing defects. In contrast, the HME-derived formulations had rougher surfaces with more printing defects, probably due to the quality of the manufactured filaments used for printing. However, geometrical defects were not visible to the naked eye and thus are not likely to affect patient compliance. The geometry of the channelled cpKVA150 spherical mini-tablets is more complex and consists of 7 internal channels within a 6 mm diameter sphere, which affected the quality of the printed geometry (Figure 4). The diameter of the commercial filaments loaded by PD was 1.75 mm (± 0.05 mm),

which is within the specification limits required for the employed 3D printer. However, higher variability was observed in the diameter of the in-house manufactured filaments (ranging from 1.46 – 1.57 mm), which can explain the larger morphological defects (Supplementary material, table S1 for diameters). The layer height of the EC-based formulations was 2-fold higher than PD and KVA-based formulations. EC-based filaments showed the highest deviation from the specification limit in terms of filament diameter, hampering the printing process. The layer height was increased to ensure a better flow of the molten polymer inside the printer. However, the higher the layer height, the higher the risk of losing resolution and altered surface area during printing. When higher layer heights were selected for the HME filaments, the extruded mixture as printed was not homogenous. Additionally, the density of the PD loaded filament was 2-3 fold higher than that obtained by HME, which is explained by the porous structure of the latter. This also impacted on the quality of the finished product considering the small size of the spherical mini-tablets (6 mm in diameter). The final weight of the printed mini-tablets was 3-6 times greater when printed from PD filaments (Supplementary material, Table S1) compared to HME mini-tablets. The porous structure observed in some of the extruded filaments is likely a result of lack of structural integrity and entrapped air due to the lack of a venting unit in the extruder used for their preparation. However, at greater magnifications, some crystals were observed on the surface of the printed mini-tablets, indicating either deposition of crystalline material on the surface or crystallisation post-processing.

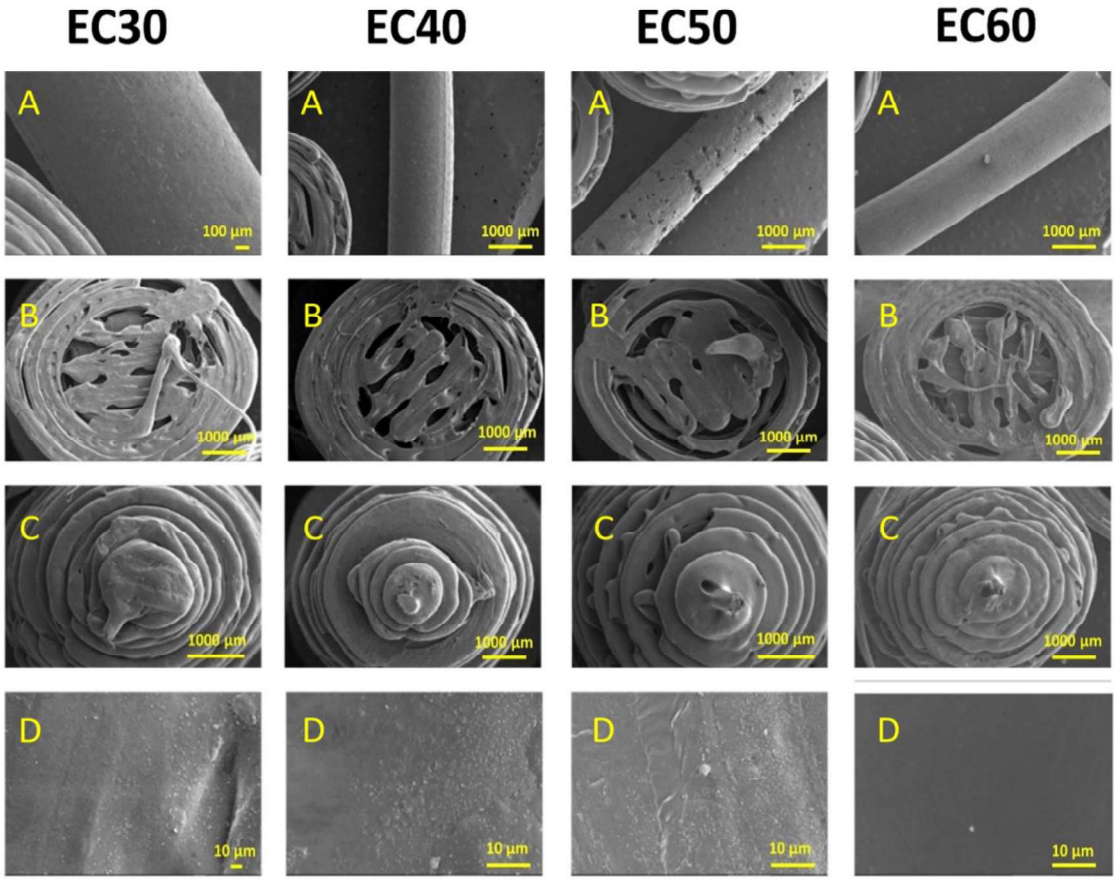

Figure 3: SEM micrographs for the EC30, EC40, EC50 and EC60 formulations containing EC as excipient. Key; A: loaded filaments, B: Mini-tablets printed up to 50% of total geometry, C: Fully printed mini-tablets and D: Surface of the mini-tablets.

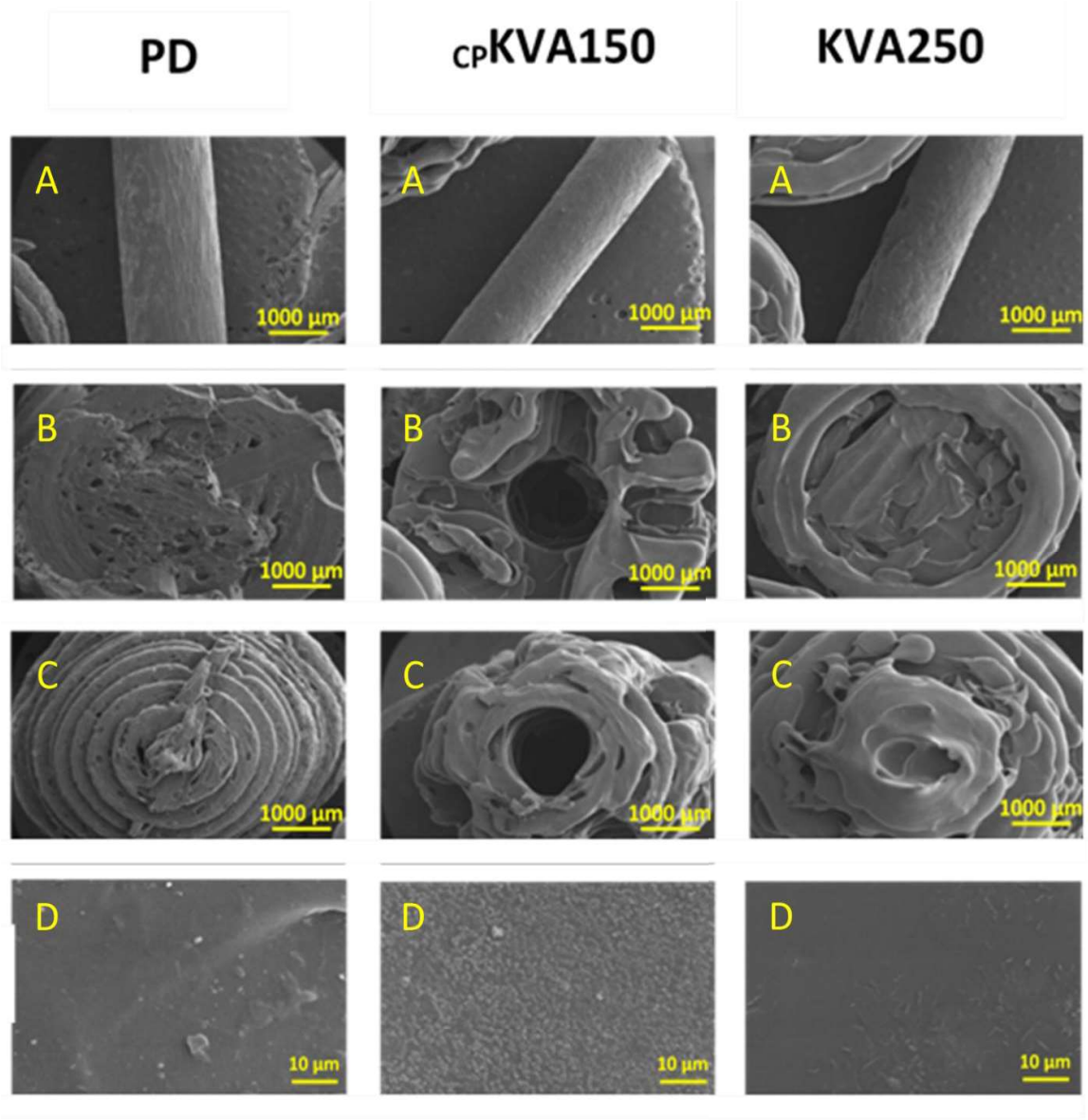

Figure 4: SEM micrographs for the PD formulation, cpKVA150 formulation and KVA250 formulation. Key: A: Loaded filaments, B: Mini-tablets printed up to 50%% of total geometry; C: Fully printed mini-tablets D: Mini-tablet surface morphology.

3.2. Friability and hardness test

For comparison purposes, the physical strength was evaluated for PD and EC50 formulations. Friability tests indicated no weight loss for the mini-tablets and filaments prepared by the PD method, while no defects were visible at the end of the friability tests for either the mini-tablets

or the filaments. However, 0.3% weight loss was observed for EC50 mini-tablets. The average crushing force is summarised in table 3. The EC50 HME mini-tablets were 35-fold more fragile than the PD mini-tablets, which is expected due to the lower printing accuracy and design integrity of the EC50 mini-tablets. Commercially available filaments (i.e. the hydrosupport filament used to prepare the PD Mini-tablets) resulted in better resolution prints with greater hardness.

Table 3: Friability and hardness of the PD formulation versus the EC50 HME formulation (n=3). Key; SD: standard deviation

Formulation	Physical form	Friability (% weight loss)	Hardness in Newton (± SD)
PD	Filaments	0.0	413.5 ± 0
	Mini-tablets	0.0	403.1 ± 14.37
EC50	Filaments	0.0	223.1 ± 0.11
	Mini-tablets	0.3 ± 0.08	11.4 ± 8.01

3.3.Content uniformity and drug loading

After PD optimisation, the highest achieved NFD loading was 4% compared to loadings of more than 50% achieved for the HME filaments. However, the homogeneity of the filaments and printed mini-tablets produced by PD was better (4.3 and 7.9% RSD respectively) than those obtained by HME (8.1 and 11.2% RSD respectively). The larger variability observed for HME filaments can be explained by several factors. It is well-known that reaggregation and de-mixing due to in melt viscosity differences and intrinsic changes in flow dynamics can often occur in a single-screw extruder. Also, it is more difficult to achieve an accurate diameter for the filaments during HME, resulting in mini-tablets with greater weight and drug loading variability. HME manufactured filaments had a diameter ranging from 1.45-1.57 mm, while a diameter of 1.75 ± 0.05 mm is recommended for printing; this resulted in lower printing quality. Regarding the drug degradation during the printing process (i.e. in processing the filament into mini-tablets), a similar loss of NFD was observed for both methods (6.7-8.5%), which is attributed to the choice of printing temperature that was similar for both PD and HME loaded filaments (Table 4).

Table 4: Drug loading and content uniformity results for the different methods. Key: SD, standard deviation.

Composition	Drug loading (±SD)		Mean drug loss due to 3D printing
	Filaments	Mini-tablets	
PD	4.00 ± 0.17 %	3.66 ±0.29 %	8.50 ± 3.05 %
EC50	53.47 ± 4.31 %	49.86 ± 5.56 %	6.75 ± 3.79 %

3.4. Solid State characterisation

PXRD

PXRD analysis of the raw materials revealed that NFD and PEG 4000 were highly crystalline (Fig. 5A). The crystallinity of the physical mixtures can be attributed mainly to NFD and PEG 4000 and partially to ethylcellulose and magnesium stearate which also exhibited Bragg peaks but of lower intensity compared to NFD and PEG 4000 (Fig. 5B). The PD formulation did not exhibit any Bragg peaks, probably indicating that the NFD is in the amorphous state. However, we need to bear in mind the lower loading of NFD in PD filaments.

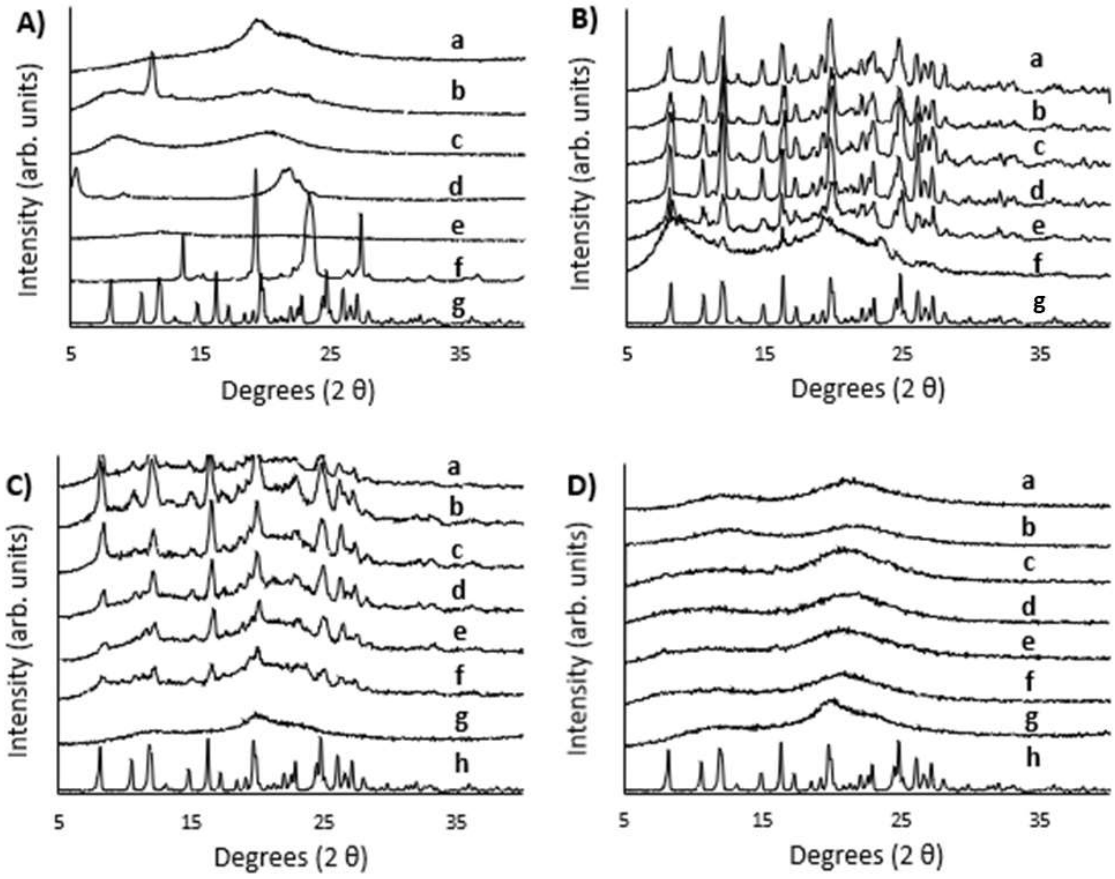

Figure 5. PXRD analysis. Key: A) Unprocessed materials; a) Hydrosupport filament b) Ethylcellulose, c) Hydroxypropyl cellulose, d) Magnesium stearate, e) Kollidon VA 64, f) Polyethylene glycol 4000 and g) NFD. B) Physical mixtures; a) KVA250 formulation, b) cpKVA150 formulation, c) EC60 formulation, d) EC50 formulation, e) EC40 formulation, f) EC30 formulation and g) NFD. C) Filaments: a) KVA250 , b) cpKVA150, c) EC60, d) EC50, e) EC40, f) EC30 and g) PD and h) NFD; D) 3D printed mini-tablets: a) KVA250 , b) cpKVA150, c) EC60, d) EC50, e) EC40, f) EC30 g) PD and h) NFD.

HME filaments demonstrate lower intensity Bragg peaks than the equivalent physical mixtures and this was more pronounced for filaments containing KVA64 compared to the EC based filaments (Fig. 5C). The lower Tg of KVA64 compared to EC allows for better interaction with NFD at the processing temperatures utilised, which explains the lower intensity peaks. The 3D printing process results in largely PXRD amorphous mini-tablets likely due to the higher temperatures used for printing, which are above the melting point of the NFD compared to the temperatures employed during HME (~ 60-80 °C less). Additionally, printing was performed at low speed to ensure higher resolution (Fig. 5D). Small Bragg peaks were found for EC60, EC50, and EC40 corresponding to NFD (indicating less than 5% crystallinity), but not for KV64-based formulations. NFD and KVA64 have more similar Hansen solubility parameters compared to NFD and EC, which explains the greater miscibility of NFD in the KVA64 polymeric matrices (Archer, 1991; Cerda et al., 2020; Kolter and Gryczke, 2012).

Differences in the PXRD diffractograms were observed between the surface and the inner core of the mini-tablets prepared with EC (Fig. S1, supplementary material). This is likely attributed to a phase separation between NFD and polymer and hence, the higher susceptibility of NFD amorphous domains to moisture which triggers the crystallisation of the NFD localised in the outer domains of the mini-tablet. However, 3D printed materials are very dense with low porosity, which limits the permeability of water molecules to the inner core of the printed mini-tablets preventing the crystallisation of amorphous NFD. This observation is further supported with dynamic vapour soprtion (DVS) data (Section 4.7**).**

Thermogravimetric analysis

TGA analysis revealed that the physical mixtures, filaments, and mini-tablets were thermally stable up to 230 °C (Fig. 6). The temperatures selected during HME and 3D printing were below 230 °C to limit thermal degradation during manufacturing of 3D printed NFD dosage forms. In all the formulations, the residual water content was below 1.3%, which is necessary to ensure a longer shelf life of the formulations.

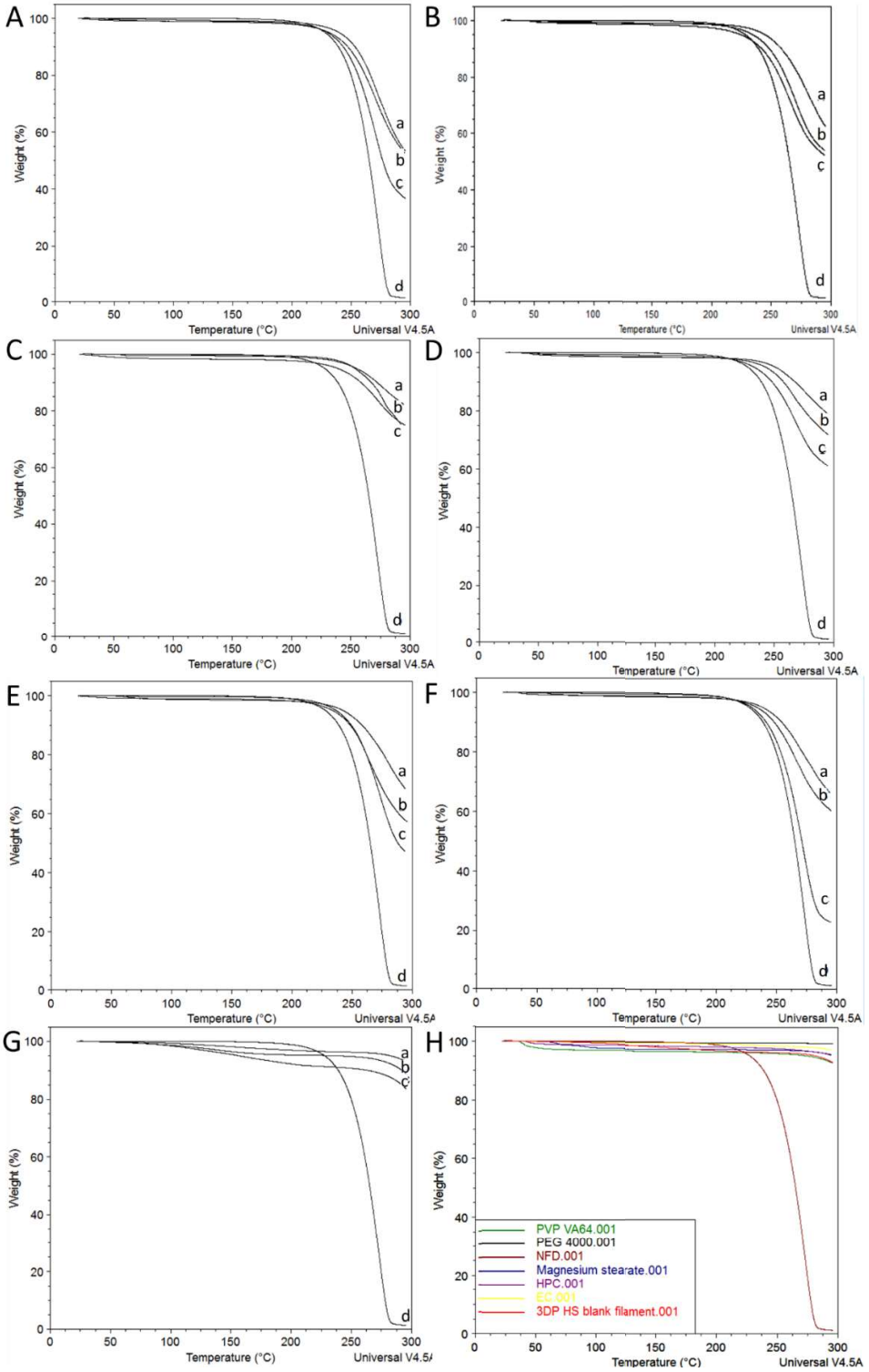

Figure 6. TGA curves for cpKVA150 (A): Mini-tablet (a), filament (b), PM (c), NFD (d). KVA250 (B): Mini-tablet (a), PM (b), filament (c), NFD (d). EC30 (C): PM (a), Mini-tablet (b), filament (c), NFD (d); EC40 (D): Mini-tablet (a), filament (b), PM (c), NFD (d); EC50 (E): Mini-tablet (a), filament (b), PM (c), NFD (d); EC60 (F): Mini-tablet (a), filament (b),

PM (c), NFD (d); PD (G): HS blank filament (a), Mini-tablet (b), loaded filament (c), NFD (d). Unprocessed materials (H).

Differential scanning calorimetry

Unprocessed NFD showed a sharp endothermic event at 173.0 ± 1.0 °C corresponding to the melting of the drug with a heat of fusion of 112.5 ± 0.8 J/g, (Fig 7A-a). Unprocessed PEG 4000 also exhibited a sharp melting event at 60.0 ± 1.0 °C (Fig 7H-a). The Tg for the KVA64 and EC was 101 °C and 127 °C respectively, which is similar to previous reported values (Kolter and Gryczke, 2012; Lai et al., 2010). Bearing in mind the XRD results which indicated the largely amorphous nature of all printed mini-tablets, it is apparent that NFD recrystallises during the DSC heating ramp of the mini-tablets printed from HME filaments (Fig.7A-7F). Based on the heat of fusion of NFD and the theoretical total content of NFD within each mini-tablet formulation, the percentage of the drug that recrystallised during the DSC run was calculated. The amount of crystalline NFD in the PD formulation was below the quantification limit (Fig. 7H). In the other systems, the lowest percentage of crystalline NFD was found in the KVA250 formulation followed by $_{CP}$KVA150 (supplementary material, table S2). EC-based formulations exhibited a higher fraction of recrystallised NFD, ranging from 50-63%. The lower crystalline content in KVA formulations may be explained by the higher miscibility with the drug and the lower Tg of the PVPVA64 compared to EC based formulations.

Melting point depression of NFD occurred in all formulations indicating that NFD is partially solubilised within the excipient matrix. A single Tg was observed for all the mini-tablet formulations (supplementary data, table S3, Fig S2) which is close to the Tg of the amorphous NFD obtained by melt quench (data not shown). This indicates that a homogenous amorphous domain is formed when interacting with the polymeric excipients. However, the low value of the Tg indicates that it is not a highly stable amorphous formulation, which can explain the crystallisation upon exposure to high relative humidity (DVS data shown in section 4.7), or on heating in the DSC. This behaviour has been associated with miscible polymer systems that exhibit monotonic negative deviations from the predictions of the mass- and volume-additivity (Fox) rules (Kalogeras and Brostow, 2009). This behaviour is usually attributed to blends with prevailing conformational entropic effects, due to the weakening of the interactions between, in this case, NFD and the polymer chain segments (see FTIR section).

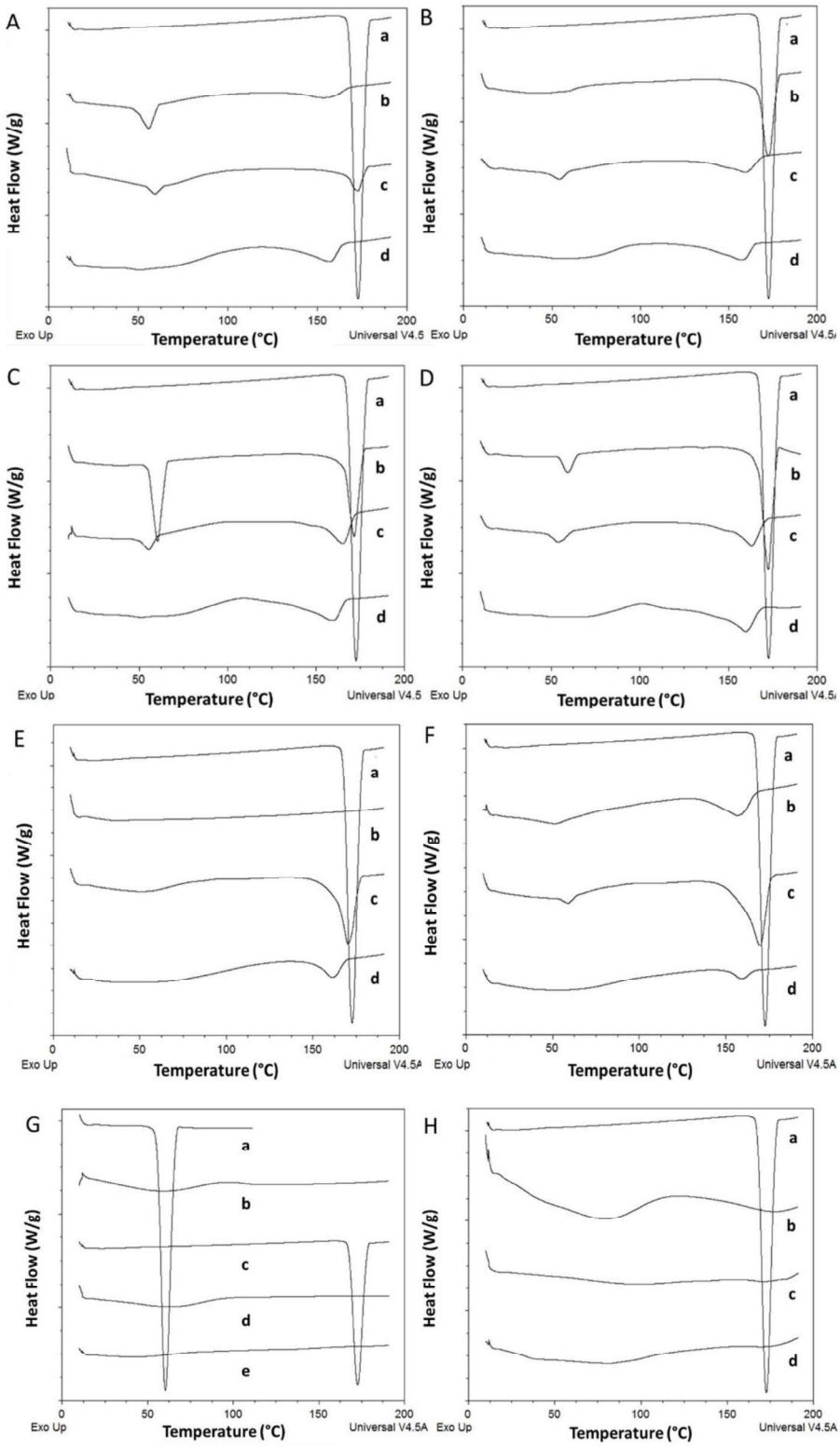

Figure 7. DSC thermograms of the unprocessed materials, physical mixtures (PM), filaments and 3D printed mini-tablets. Key: EC30 (A), EC40 (B), EC50 (C), EC60 (D), cpKVA150 (E), KVA250 (F), unprocessed materials (G) and PD (H). Within the graphs(A-F): NFD unprocessed material (a), PM (b), filament (c) and mini-tablet (d). For graph (G):

PEG 4000 (a), KVA64 (b), NFD (c), HPC (d) and EC (e). For graph (H); NFD unprocessed material (a), Hydrosupport filament (b), NFD loaded hydrosupport filament (c) and mini-tablet (d).

Fourier Transform Infrared Spectroscopy (FTIR)

FTIR spectra revealed H-bond interactions between NFD and the excipients (Fig. 8). Shifts were observed in the carbonyl (C=O stretching at 1679 cm^{-1}) and the C-O (1225 cm^{-1}) functional groups of NFD after co-processing by HME and after 3D printing. None of these shifts were present in the physical mixtures (PM). Shifts were more prominent in the KVA64-based formulations compared to the EC-based formulations indicating stronger API-polymer interactions and better miscibility. Similar shifts were observed in the KVA250 formulation compared to the $_{CP}$KVA150. Amongst the EC-based formulations, strongest shifts were observed in the EC30 formulation, for which the ratio of total excipients to NFD was the greatest. Finally, filaments and 3D printed mini-tablets showed broader bands, possibly due to the greater amorphous nature of the systems compared to the physical mixtures and unprocessed NFD.

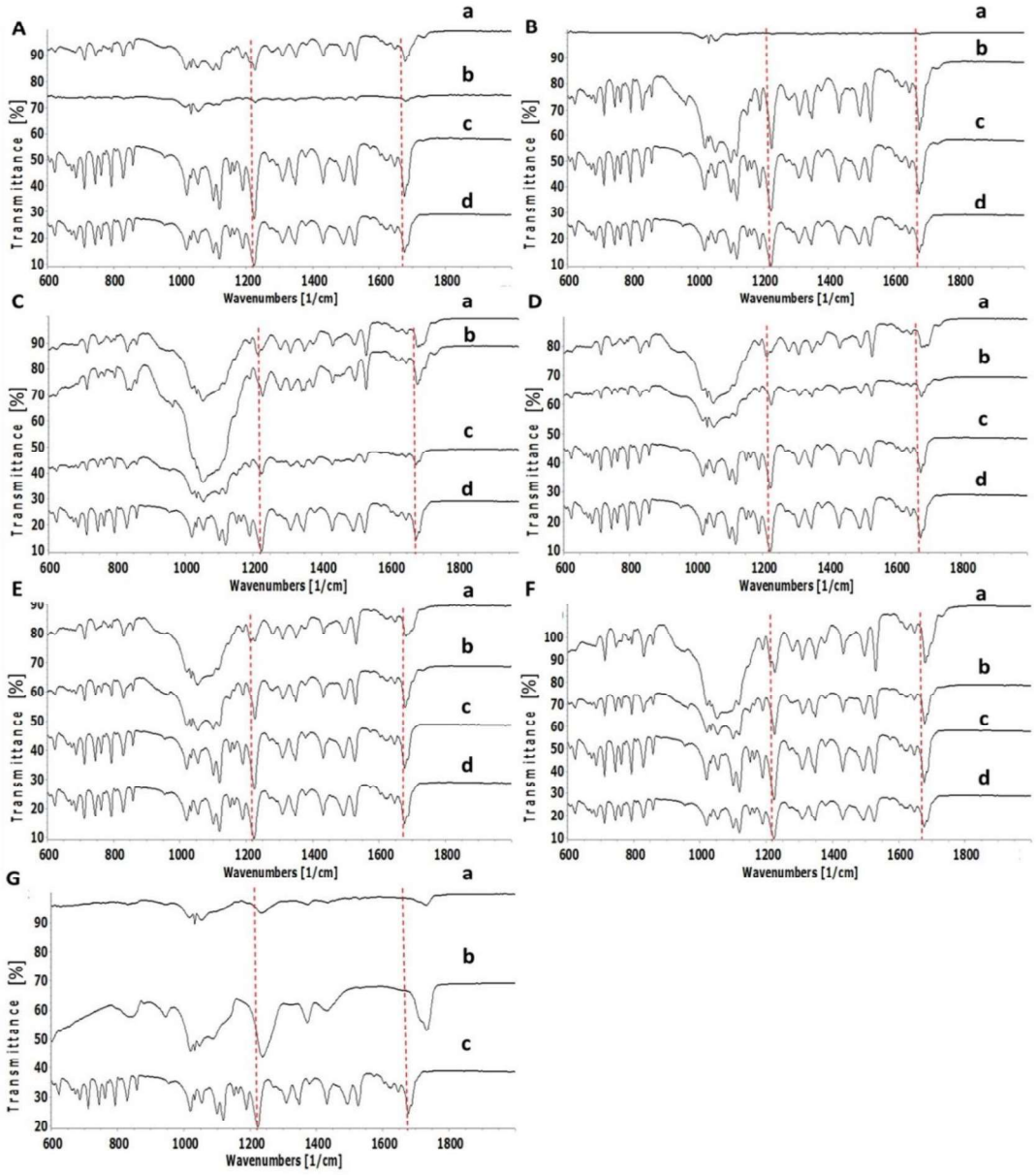

Figure 7. FTIR spectra of the physical mixtures, filaments, and 3D printed mini-tablets. Key: cpKVA150 (A), KVA250 (B), EC30 (C), EC40 (D), EC50 (E), EC60 (F), PD (G). Within the graphs (A-F): Mini-tablet (a), filament (b), PM (c) and unprocessed NFD (d). For graph (G); Mini-tablet (a), loaded HS filament (b) and unprocessed NFD (c).

3.5. Dissolution studies

As crystalline NFD has a low aqueous solubility, dissolution studies were performed in media containing sodium lauryl sulphate to ensure sink conditions. A markedly different dissolution profile was observed for the two commercially marketed NFD tablets (Fig. 9). Adalat Oros is an osmotic system consisting of a semi-impermeable barrier created mainly by cellulose acetate

and a dual reservoir with sodium chloride and NFD amongst other excipients (Liu et al., 2003). The compartment with sodium chloride, upon wetting, increases the osmotic pressure of the system forcing the NFD contained in the other compartment to be slowly released across the pore located at the surface of the tablet. This behaviour results in a zero-order release (R^2= 0.9874) as clearly observed in figure 9. In contrast, Stada tablets (even though they are retard formulations) were rapidly disintegrated into smaller fragments from which the NFD was released. The 3D printed mini-tablets prepared using PD filaments showed a sustained release over 6 h and behaved like monolithic matrices from which the drug diffused into the liquid media matching the results obtained by other authors (Cerda et al., 2020). The best fitted dissolution kinetic model for Stada tablets and PD mini-tablets was Higuchi (R^2= 0.8859) and Korsmeyer-Peppas (R^2= 0.9878), respectively (Supplementary data, Table S4).

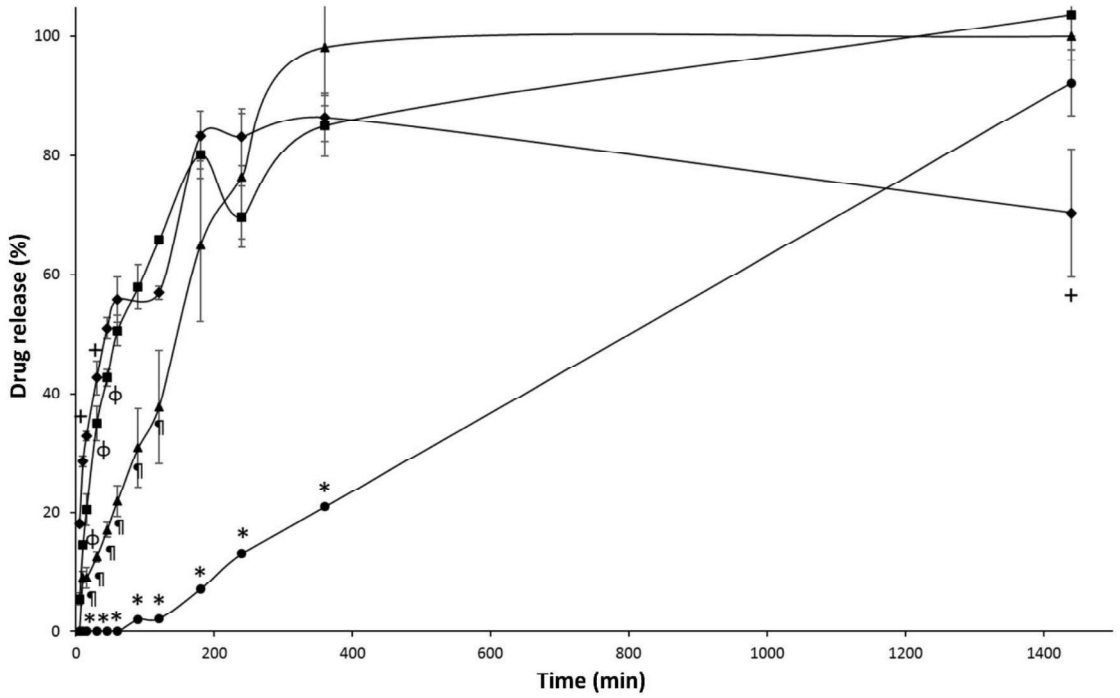

Figure 8: Dissolution profile for the PD formulation (-▲-) compared to unprocessed NFD (-♦-) and commercially marketed NFD tablets: Adalat OROS 30 mg (-●-) and Nifedipine STADA retard 20 mg (-■-). Key: *p<0.05 Adalat OROS vs. all other formulations (incl. t=5 and t=10); ¶p<0.05 PD vs. all other formulations (incl. t=5 and t=10); +p<0.05 raw NFD vs. all other formulations (incl. t=5 to t=15) and Φp<0.05 STADA vs. all other formulations (incl. t=5 to t=15).

A dissolution study was also performed for the HME-based mini-tablets (Fig. 10). In all cases, a biphasic release was observed, with two apparent zero-order release phases. The main excipient used in the formulation played a key role in the speed and extent of the NFD release. The dissolution profile of the KVA-based mini-tablets showed a faster drug-release profile than EC-based formulations. The channelled $_{cp}$KVA150 mini-tablets had the fastest and most complete drug-release from all formulations, which can be attributed to the greater surface area (1.6-fold greater than non-channelled mini-tablets of KVA) and the composition. The release profile of KVA formulations more closely mimicked the Adalat Oros profile, but with a greater

burst release observed in SGF over the first two hours. The dissolution profile from the EC-based formulations was slow and incomplete. A higher percentage of NFD within the EC matrix did not result in a faster release and the EC60 formulation showed the poorest release profile. However, the EC50 formulation showed a slightly better dissolution performance compared to other EC-based formulations. No statistically significant differences were observed between the dissolution profiles of EC50 and cpEC50 formulations (Supplementary data, Fig S3). This demonstrates the importance of the suitable selection of the excipient over the geometry when designing sustained release solid dosage forms.

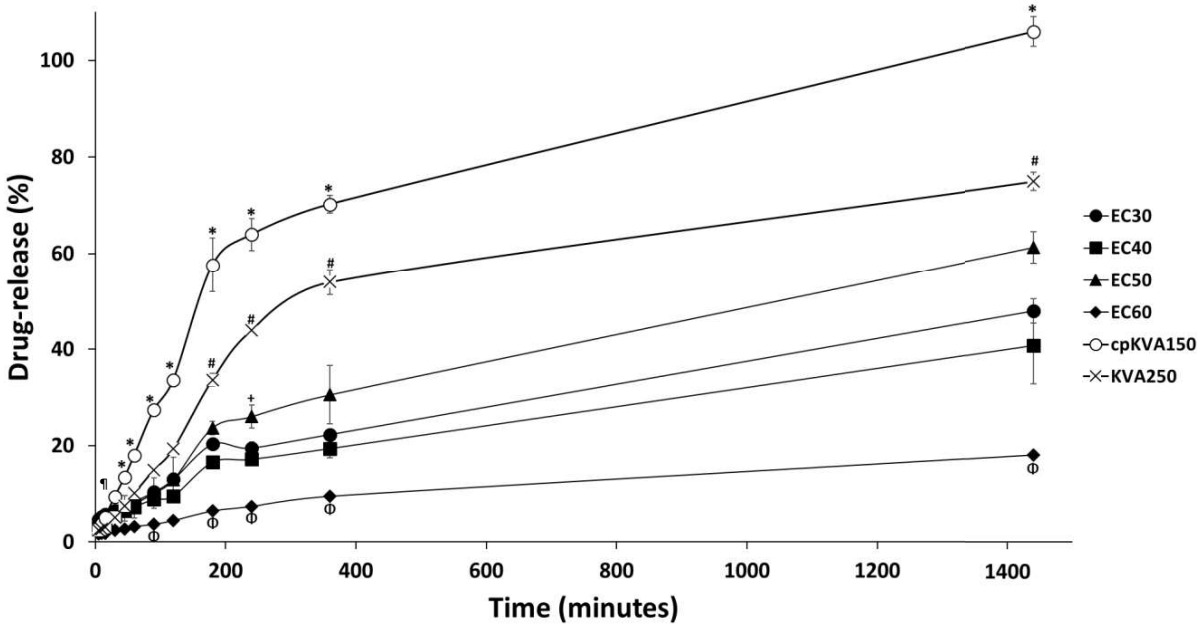

Figure 9: Drug-release profiles for all HME formulations. Key: *: p<0.05 cpKVA150 vs. all other formulations; #: p<0.05 KVA250 vs. all other formulations; +: p<0.05 EC50 vs. all other formulations; Φ: p<0.05 EC60 vs. all other formulations (incl. t=5 to t=15) and ¶: p<0.05 EC30 vs. all other formulations (t=5, t=10).

3.6. Multivariate analysis of the effect of excipients on the dissolution profile

To optimize the drug release profile, the impact of NFD and the three key excipients employed in the manufacturing of the HME-based tablets (EC, KVA64, HPC) on the percentage of drug released at 6 hours was evaluated (Fig. 5). PCA analysis showed an inverse correlation between EC and KVA64 content on the NFD drug release. The same correlation was observed by multi linear regression (MLR) analysis, corroborating that fact that KVA64 had a statistically significant positive effect on the NFD release ($p=0.0015$), while EC had a statistically significant negative impact ($p=0.0181$).

The percentage of HPC and NFD did not show a statistically significant correlation with the NFD release ($p>0.05$). This explains why EC-based mini-tablets with a wide range of NFD content (30-60%) did not show any correlation in terms of NFD release. Even though a limited number of formulations was used to feed the model, a good PLS correlation (high $R^2> 0.99$

and a low Mean Square Root Error <0.8) was found between the type and percentage of excipient with the NFD released at 6 h (Supplementary material, Fig. S4).

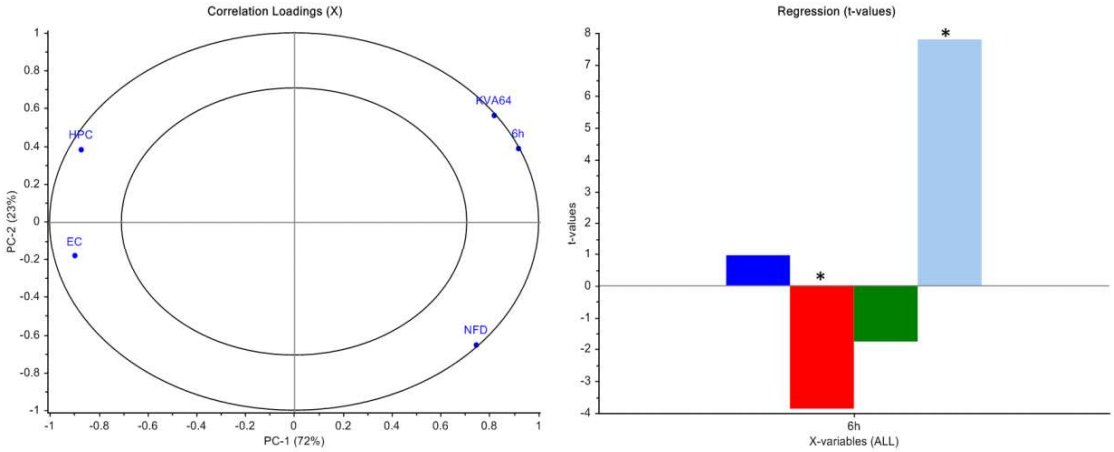

Figure 10: Principal component analysis represented by the correlation loading plot (left) and MLR analysis represented as T-values (right). Key: NFD (dark blue), EC (red), HPC (green), KVA64 (light blue). Statistically significant differences are depicted as *p<0.05.

3.7. Dynamic vapour sorption (DVS)

DVS analysis was performed to compare the adsorption moisture profile of the 3D printed mini-tablets (with 50% NFD) that contained either EC or KVA64 in their matrix. Moisture sorption isotherms showed a similar profile for both formulations up to 60% RH (Fig. 11). There is a gradual increase in water uptake (~2%) for both formulations. However, markedly different behaviour in the sorption profile was observed above 70% RH. The KVA64 mini-tablet showed a gradual increase in water uptake until 90% RH, while the EC50 mini-tablet showed a decrease in mass at 70-80 % RH associated with drug crystallisation. PXRD analysis was performed after DVS and confirmed the crystallisation of the NFD under high RH conditions in the mini-tablet with EC (data not shown). Regarding the desorption cycle, a large hysteresis was observed in the KVA64 mini-tablet, which can be linked to the formation of small cavities and pores during the cooling of the extrudates, where water can condense, slowing down the desorption process. The combination of PXRD, DSC, TGA, and DVS data led to the conclusion that the formulations containing KVA64 as polymeric matrix represent a more physically stable amorphous system compared with the EC-based formulations.

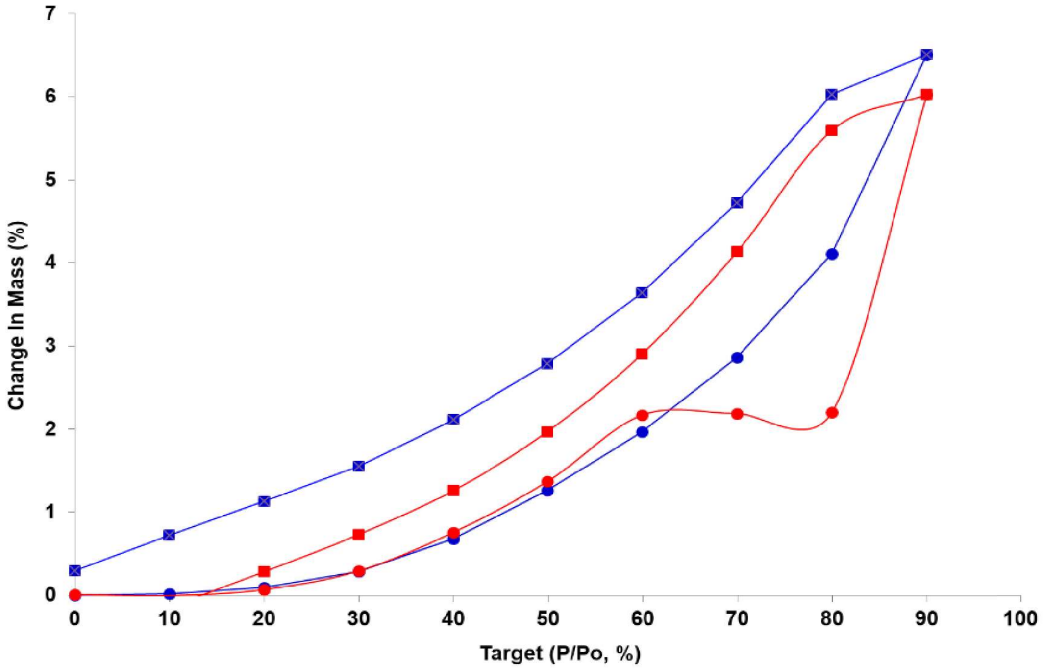

Figure 11: Moisture adsorption isotherms for KVA50 (blue line) and EC50 (red line) mini-tablets. Key: Circles represent the sorption cycle and squares represent the desorption cycle.

4. Discussion

In this work we have demonstrated that the release profile of a poorly water-soluble API (NFD) can be tailored using 3D printing with drug-loaded filaments produced by PD or HME and we demonstrated for the first time the manufacture of channelled mini-tablets with enhanced surface area. The major drawbacks of PD loaded filaments are that the maximum drug loading achieved was only 4% and the process is lengthy. HME-based filaments demonstrated more than 13-fold higher loading compared to PD filaments. Filaments loaded with up to 60% NFD were successfully manufactured by HME. However, HME is more complicated to implement in clinical practice within hospitals, for example, while passive diffusion, especially for potent drugs, could be more easily achieved. 3D printers with a direct powder extrusion module can be an alternative to avoid the need of creating a printable filament through HME. A closer collaboration between industry and hospitals will be required to enable the clinical translation of these 3D printed personalised solid dosage forms based on HME filaments.

A greater resolution of the printed mini-tablets was obtained when using PD loaded commercial filaments as HME filaments were more heterogeneous in diameter and were more porous due to the extrusion process. The latter issue can be easily overcome using high specification industrial hot melt extruders with twin co-rotating screws and a ventilation unit to remove generated air during the mixing and the melting within the extruder. The use of a highly concentrated masterbatch use and intermediary products can be other approaches.

Loaded filaments were utilised to prepare 6 mm spherical mini-tablets.

Mini-tablets are easier to combine within a capsule avoiding potential physicochemical interactions between different active pharmaceutical ingredients, while they also allow versatility in the administered dose. A size 0 capsule was selected as three mini-tablets can fit within it. This allows a greater versatility to manufacture tailored oral dosage forms either by increasing the dose of NFD per capsule or combining different APIs (fixed-dose combinations (Fernandez-Garcia et al., 2020)) within the same capsule to treat multiple pathologies such as hypertension, hypercholesterolemia and diabetes. However, mini-tablets are more challenging to 3D print considering the smaller dimensions compared to larger tablets especially when including additional intricate channels to increase surface area.

We were also able to determine which, between geometry and composition, seems the most important consideration for 3D printing these dosage forms. Initially, mini-tablets with different diameters were 3D printed. However, the increase in surface area was limited and the impact on dissolution was not statistically significant (data not shown). For this reason, a more complex geometry including seven internal channels was developed to increase the surface area of the mini-tablets by 1.6-fold. Several authors have shown that the geometry of the solid dosage form has a key impact on dissolution (Goyanes et al., 2015b; Sadia et al., 2018). Surprisingly, the change in geometry and the enhancement in the surface area only led to a significantly faster dissolution profile in those formulations containing KVA64, but not in those with EC. This shows that the dissolution of NFD was governed first by the composition of the mini-tablet and secondly by the geometry. EC-based formulations showed an overall hampered dissolution profile compared to the KVA-based ones. The enhancement in the surface area of the EC-based mini-tablets was not sufficient to trigger an improvement in the dissolution rate. This can be related with the formation of a gel-like layer around the mini-tablet limiting dissolution and inhibiting the effect of the greater surface area. However, those solid mini-tablets containing KVA64 show a faster dissolution rate and more complete dissolution profile, and hence, the additional increase in surface area was translated into amplified release. Based on the Hansen solubility parameters, KVA64 has better miscibility than EC with NFD. This can explain the better amorphization of the NFD within the excipient matrix, and the more stable amorphous system upon exposure to high RH leading to a single Tg composite observed by DSC. Nevertheless, a fraction of crystalline NFD remained after the 3D printing process in both types of HME formulations indicating that the manufacturing of filaments with a lower percentage of NFD will be more suitable to ensure stability over prolonged periods.

The dissolution profile of the NFD mini-tablets can be tailored when a successful geometry and composition are combined. NFD is a poorly soluble BCS Class II drug. Slow and incomplete dissolution profiles have been previously reported for 3D printed solid dosage forms, especially when high levels of hydroxypropyl methyl cellulose were used (Khaled et al., 2015). Mini-tablets prepared from PD filaments demonstrated a faster release profile matching that of NFD commercial tablets (Stada). HME mini-tablets showed a biphasic release with two zero-order phases, more closely mimicking the commercial Adalat Oros profile, especially those mini-tablets containing KVA, as the EC-based mini-tablets, resulted in an incomplete release with a slow rate. This is possibly due to the formation of a diffusion and erosion-resistant gel layer that hinders release of NFD, also limiting effects from the higher

surface area conferred by the pores. Zero-order release is clinically suitable for antihypertensives as immediate release formulations can elicit serious adverse effects, such as orthostatic hypotension, whereas a 24 h sustained release can provide the required pharmacological effect over a whole day, consequently enhancing patient compliance as only a single dose is required.

5. Conclusions

3D printing is a versatile technology providing the possibility to manufacture solid dosage forms within complex geometries, such as channelled mini-tablets, potentially with high drug-loading (up to 60%). In this work, we have shown that appropriately combining the solid dosage form composition and geometry allows us to tailor drug-release profiles according to the patient's needs. The composition of the extruded filaments has a more significant impact on dissolution than geometry. KVA-based mini-tablets exhibited a faster and more complete release than EC-based formulations showing a similar release profile to other commercially available formulations and may be easily translated into clinical practice.

Acknowledgements

AM Healy acknowledges Science Foundation Ireland grants co-funded under the European Regional Development Fund (SFI/12/RC/2275 and SFI/12/RC/2275_P2). Sejad Ayyoubi was supported with an Erasmus+ grant to undertake a placement at UCM, Madrid, Spain. This study was also partially supported by the Complutense University of Madrid (910939 Formulación y biodisponibilidad de nuevos medicamentos).

References

Archer, W.L., 1991. Determination of Hansen solubility parameters for selected cellulose ether derivatives. Ind. Eng. Chem. Res. 30, 2292-2298.

Awad, A., Fina, F., Trenfield, S.J., Patel, P., Goyanes, A., Gaisford, S., Basit, A.W., 2019. 3D Printed Mini-tablets (Miniprintlets): A Novel, Multi-Drug, Controlled Release Platform Technology. Pharmaceutics 11.

Awad, A., Trenfield, S.J., Gaisford, S., Basit, A.W., 2018a. 3D printed medicines: A new branch of digital healthcare. International journal of pharmaceutics 548, 586-596.

Awad, A., Trenfield, S.J., Goyanes, A., Gaisford, S., Basit, A.W., 2018b. Reshaping drug development using 3D printing. Drug Discov Today 23, 1547-1555.

Cavallari, C., Ternullo, S., Tarterini, F., Fini, A., 2016. Release Problems for Nifedipine in the Presence of Soluplus. Journal of Pharmacy & Pharmaceutics 3, 70-82.

Cerda, J.R., Arifi, T., Ayyoubi, S., Knief, P., Ballesteros, M.P., Keeble, W., Barbu, E., Healy, A.M., Lalatsa, A., Serrano, D.R., 2020. Personalised 3D Printed Medicines: Optimising Material Properties for Successful Passive Diffusion Loading of Filaments for Fused Deposition Modelling of Solid Dosage Forms. Pharmaceutics 12.

Costa, P., Sousa Lobo, J.M., 2001. Modeling and comparison of dissolution profiles. European journal of pharmaceutical sciences : official journal of the European Federation for Pharmaceutical Sciences 13, 123-133.

Da Silva Leite, R., De Oliveira Macedo, R., Torres, S.M., Batista, C.C.N., De Oliveira Baltazar, L., Neto, S.A.L., De Souza, F.S.J.J.o.T.A., Calorimetry, 2013. Evaluation of thermal stability and parameters of dissolution of nifedipine crystals. 111, 2117-2123.

Elbadawi, M., Gustaffson, T., Gaisford, S., Basit, A.W., 2020a. 3D printing tablets: Predicting printability and drug dissolution from rheological data. International journal of pharmaceutics 590, 119868.
Elbadawi, M., Muniz Castro, B., Gavins, F.K.H., Ong, J.J., Gaisford, S., Perez, G., Basit, A.W., Cabalar, P., Goyanes, A., 2020b. M3DISEEN: A novel machine learning approach for predicting the 3D printability of medicines. International journal of pharmaceutics 590, 119837.
Fanous, M., Gold, S., Muller, S., Hirsch, S., Ogorka, J., Imanidis, G., 2020. Simplification of fused deposition modeling 3D-printing paradigm: Feasibility of 1-step direct powder printing for immediate release dosage form production. International journal of pharmaceutics 578, 119124.
Femmer, T., Flack, I., Wessling, M., 2016. Additive Manufacturing in Fluid Process Engineering. 88, 535-552.
Fernandez-Garcia, R., de Pablo, E., Ballesteros, M.P., Serrano, D.R., 2017. Unmet clinical needs in the treatment of systemic fungal infections: The role of amphotericin B and drug targeting. International journal of pharmaceutics 525, 139-148.
Fernandez-Garcia, R., Prada, M., Bolas-Fernandez, F., Ballesteros, M.P., Serrano, D.R., 2020. Oral Fixed-Dose Combination Pharmaceutical Products: Industrial Manufacturing Versus Personalized 3D Printing. Pharmaceutical research 37, 132.
Fina, F., Goyanes, A., Rowland, M., Gaisford, S., A, W.B., 2020. 3D Printing of Tunable Zero-Order Release Printlets. Polymers (Basel) 12.
Gajendran, J., Kramer, J., Shah, V.P., Langguth, P., Polli, J., Mehta, M., Groot, D.W., Cristofoletti, R., Abrahamsson, B., Dressman, J.B., 2015. Biowaiver Monographs for Immediate-Release Solid Oral Dosage Forms: Nifedipine. J Pharm Sci 104, 3289-3298.
Gioumouxouzis, C.I., Tzimtzimis, E., Katsamenis, O.L., Dourou, A., Markopoulou, C., Bouropoulos, N., Tzetzis, D., Fatouros, D.G., 2020. Fabrication of an osmotic 3D printed solid dosage form for controlled release of active pharmaceutical ingredients. European journal of pharmaceutical sciences : official journal of the European Federation for Pharmaceutical Sciences 143, 105176.
Goyanes, A., Allahham, N., Trenfield, S.J., Stoyanov, E., Gaisford, S., Basit, A.W., 2019. Direct powder extrusion 3D printing: Fabrication of drug products using a novel single-step process. International journal of pharmaceutics 567, 118471.
Goyanes, A., Buanz, A.B.M., Basit, A.W., Gaisford, S., 2014. Fused-filament 3D printing (3DP) for fabrication of tablets. International Journal of Pharmaceutics 476, 88-92.
Goyanes, A., Buanz, A.B.M., Hatton, G.B., Gaisford, S., Basit, A.W., 2015a. 3D printing of modified-release aminosalicylate (4-ASA and 5-ASA) tablets. European Journal of Pharmaceutics and Biopharmaceutics 89, 157-162.
Goyanes, A., Robles Martinez, P., Buanz, A., Basit, A.W., Gaisford, S., 2015b. Effect of geometry on drug release from 3D printed tablets. International journal of pharmaceutics 494, 657-663.
Harvey, A., Brand, A., Holgate, S.T., Kristiansen, L.V., Lehrach, H., Palotie, A., Prainsack, B., 2012. The future of technologies for personalised medicine. N Biotechnol 29, 625-633.
Isreb, A., Baj, K., Wojsz, M., Isreb, M., Peak, M., Alhnan, M.A., 2019. 3D printed oral theophylline doses with innovative 'radiator-like' design: Impact of polyethylene oxide (PEO) molecular weight. International journal of pharmaceutics 564, 98-105.
Januskaite, P., Xu, X., Ranmal, S.R., Gaisford, S., Basit, A.W., Tuleu, C., Goyanes, A., 2020. I Spy with My Little Eye: A Paediatric Visual Preferences Survey of 3D Printed Tablets. Pharmaceutics 12.
Kalogeras, I.M., Brostow, W., 2009. Glass transition temperatures in binary polymer blends. 47, 80-95.
Khaled, S.A., Burley, J.C., Alexander, M.R., Yang, J., Roberts, C.J., 2015. 3D printing of tablets containing multiple drugs with defined release profiles. International journal of pharmaceutics 494, 643-650.
Kolter, K., Gryczke, A., 2012. Hot-Melt Extrusion with BASF Pharma Polymers Extrusion Compendium, 2nd revised and enlarged edition ed.

Konta, A.A., Garcia-Pina, M., Serrano, D.R., 2017. Personalised 3D Printed Medicines: Which Techniques and Polymers Are More Successful? Bioengineering 4.
Lai, H.L., Pitt, K., Craig, D.Q., 2010. Characterisation of the thermal properties of ethylcellulose using differential scanning and quasi-isothermal calorimetric approaches. International journal of pharmaceutics 386, 178-184.
Lao, L.L., Peppas, N.A., Boey, F.Y., Venkatraman, S.S., 2011. Modeling of drug release from bulk-degrading polymers. International journal of pharmaceutics 418, 28-41.
Liu, X., Chen, D., Zhang, R., 2003. Evaluation of Monolithic Osmotic Tablet System for Nifedipine Delivery In Vitro and In Vivo. Drug Development and Industrial Pharmacy 29, 813-819.
Mamani, P.L., Ruiz-Caro, R., Veiga, M.D., 2012. Matrix tablets: the effect of hydroxypropyl methylcellulose/anhydrous dibasic calcium phosphate ratio on the release rate of a water-soluble drug through the gastrointestinal tract I. In vitro tests. AAPS PharmSciTech 13, 1073-1083.
Maniruzzaman, M., Boateng, J.S., Snowden, M.J., Douroumis, D., 2012. A Review of Hot-Melt Extrusion: Process Technology to Pharmaceutical Products %J ISRN Pharmaceutics. 2012, 9.
Matji, A., Donato, N., Gagol, A., Morales, E., Carvajal, L., Serrano, D.R., Worku, Z.A., Healy, A.M., Torrado, J.J., 2019. Predicting the critical quality attributes of ibuprofen tablets via modelling of process parameters for roller compaction and tabletting. International journal of pharmaceutics 565, 209-218.
Nasereddin, J.M., Wellner, N., Alhijjaj, M., Belton, P., Qi, S., 2018. Development of a Simple Mechanical Screening Method for Predicting the Feedability of a Pharmaceutical FDM 3D Printing Filament. Pharmaceutical research 35, 151-151.
Nukala, P.K., Palekar, S., Patki, M., Patel, K., 2019. Abuse Deterrent Immediate Release Egg-Shaped Tablet (Egglets) Using 3D Printing Technology: Quality by Design to Optimize Drug Release and Extraction. AAPS PharmSciTech 20, 80.
Ong, J.J., Awad, A., Martorana, A., Gaisford, S., Stoyanov, E., Basit, A.W., Goyanes, A., 2020. 3D printed opioid medicines with alcohol-resistant and abuse-deterrent properties. International journal of pharmaceutics 579, 119169.
Pereira, B.C., Isreb, A., Isreb, M., Forbes, R.T., Oga, E.F., Alhnan, M.A., 2020. Additive Manufacturing of a Point-of-Care "Polypill:" Fabrication of Concept Capsules of Complex Geometry with Bespoke Release against Cardiovascular Disease. Adv Healthc Mater 9, e2000236.
Rolon, M., Serrano, D.R., Lalatsa, A., de Pablo, E., Torrado, J.J., Ballesteros, M.P., Healy, A.M., Vega, C., Coronel, C., Bolas-Fernandez, F., Dea-Ayuela, M.A., 2017. Engineering Oral and Parenteral Amorphous Amphotericin B Formulations against Experimental Trypanosoma cruzi Infections. Molecular pharmaceutics 14, 1095-1106.
Sadia, M., Arafat, B., Ahmed, W., Forbes, R.T., Alhnan, M.A., 2018. Channelled tablets: An innovative approach to accelerating drug release from 3D printed tablets. Journal of controlled release : official journal of the Controlled Release Society 269, 355-363.
Serrano, D.R., Cerda, J.R., Fernández-García, R., Pérez-Ballesteros, L.F., Ballesteros, M.P., Lalatsa, A., 2019a. Chapter 9: Market Demands in 3D Printing Pharmaceuticals Products, in: Ahmad, N., Gopinath, P., Dutta, R. (Eds.), 3D Printing Technology in Nanomedicine, pp. 165-185.
Serrano, D.R., O'Connell, P., Paluch, K.J., Walsh, D., Healy, A.M., 2016. Cocrystal habit engineering to improve drug dissolution and alter derived powder properties. The Journal of pharmacy and pharmacology 68, 665-677.
Serrano, D.R., Terres, M.C., Lalatsa, A., 2019b. Applications of 3D Printing in Cancer. Journal of 3D printed in medicine 2, 1-26.
Serrano, D.R., Walsh, D., O'Connell, P., Mugheirbi, N.A., Worku, Z.A., Bolas-Fernandez, F., Galiana, C., Dea-Ayuela, M.A., Healy, A.M., 2018. Optimising the in vitro and in vivo performance of oral cocrystal formulations via spray coating. European journal of pharmaceutics and biopharmaceutics : official journal of Arbeitsgemeinschaft fur Pharmazeutische Verfahrenstechnik e.V 124, 13-27.
Siepmann, J., Siepmann, F., 2013. Mathematical modeling of drug dissolution. International journal of pharmaceutics 453, 12-24.

Skowyra, J., Pietrzak, K., Alhnan, M.A., 2015. Fabrication of extended-release patient-tailored prednisolone tablets via fused deposition modelling (FDM) 3D printing. European Journal of Pharmaceutical Sciences 68, 11-17.
Tan, D.K., Maniruzzaman, M., Nokhodchi, A., 2019. Development and Optimisation of Novel Polymeric Compositions for Sustained Release Theophylline Caplets (PrintCap) via FDM 3D Printing. Polymers (Basel) 12.
Tiwari, R.V., Patil, H., Repka, M.A., 2016. Contribution of hot-melt extrusion technology to advance drug delivery in the 21st century. Expert opinion on drug delivery 13, 451-464.
Trenfield, S.J., Xian Tan, H., Awad, A., Buanz, A., Gaisford, S., Basit, A.W., Goyanes, A., 2019. Track-and-trace: Novel anti-counterfeit measures for 3D printed personalized drug products using smart material inks. International journal of pharmaceutics 567, 118443.
United States Pharmacopeia and National Formulary (USP 38-NF 33). General Chapters: <1216> TABLET FRIABILITY. Rockville, M.U.S.P.C.A.d., 2018. .
United States Pharmacopeia and National Formulary (USP 38-NF 33). General Chapters: <1217> TABLET BREAKING FORCE. Rockville, M.U.S.P.C.A.d.
United States Pharmacopeia and National Formulary (USP 38-NF 33). Reagents: Test Solutions. Rockville, M.U.S.P.C.A.d., 2018.
Verstraete, G., Samaro, A., Grymonpre, W., Vanhoorne, V., Van Snick, B., Boone, M.N., Hellemans, T., Van Hoorebeke, L., Remon, J.P., Vervaet, C., 2018. 3D printing of high drug loaded dosage forms using thermoplastic polyurethanes. International journal of pharmaceutics 536, 318-325.
Wilson, M., Williams, M.A., Jones, D.S., Andrews, G.P., 2012. Hot-melt extrusion technology and pharmaceutical application. Therapeutic delivery 3, 787-797.
Zhang, Y., Huo, M., Zhou, J., Zou, A., Li, W., Yao, C., Xie, S., 2010. DDSolver: An Add-In Program for Modeling and Comparison of Drug Dissolution Profiles. The AAPS Journal 12, 263-271.